Efficient reconstruction method for L1 regularization in fluorescence molecular tomography

Dong Han,[1,†] Xin Yang,[1,†] Kai Liu,[1] Chenghu Qin,[1] Bo Zhang,[2] Xibo Ma,[1] and Jie Tian[1,*]

[1]Medical Image Processing Group, Institute of Automation, Chinese Academy of Sciences, Beijing 100190, China

[2]Sino-Dutch Biomedical and Information Engineering School of Northeastern University, Shenyang 110004, China

*Corresponding author: tian@ieee.org

Received 6 July 2010; revised 23 October 2010; accepted 29 October 2010; posted 2 November 2010 (Doc. ID 131164); published 15 December 2010

Fluorescence molecular tomography (FMT) is a promising technique for *in vivo* small animal imaging. In this paper, the sparsity of the fluorescent sources is considered as the *a priori* information and is promoted by incorporating L1 regularization. Then a reconstruction algorithm based on stagewise orthogonal matching pursuit is proposed, which treats the FMT problem as the basis pursuit problem. To evaluate this method, we compare it to the iterated-shrinkage-based algorithm with L1 regularization. Numerical simulations and physical experiments show that the proposed method can obtain comparable or even slightly better results. More importantly, the proposed method was at least 2 orders of magnitude faster in these experiments, which makes it a practical reconstruction algorithm. © 2010 Optical Society of America

OCIS codes: 170.6960, 170.6280, 170.3010.

1. Introduction

Fluorescence molecular tomography (FMT) is a cost-effective method for *in vivo* small animal molecular imaging, and it has many successful applications [1–4]. Based on certain inverse mathematical models, FMT can achieve three-dimensional (3D) imaging of molecular processes noninvasively by localizing the targeted fluorescent probes. In recent years, much effort has been made in developing practical FMT reconstruction algorithms [5–8].

Fluorescence molecular tomography is an inverse problem that is severely ill posed. Therefore, to obtain meaningful solutions, some form of regularization should be incorporated to stabilize the FMT problem, which can be considered as the *a priori* information of the fluorescent probe biodistribution. When FMT is used for early detection of tumors, an important characteristic is the sparsity of the fluorescent sources. This is because tumors are usually very small and sparse at this stage [9]. Generally speaking, there are two kinds of fluorescent sources: the fluorescent protein and fluorescent probe. The fluorescent protein is produced by the transgenic tumor cells, which contain the fluorescent protein gene. The fluorescent probe is exogenous and can be used to target a specific receptor or enzyme of the tumor cell. For both cases, the fluorescent sources are around the tumor cells. Because the tumors are sparse, we can assume that the fluorescent sources have a sparsity distribution as well. Sparsity can be promoted by including the L0-norm constraint in the reconstruction. However, the FMT problem becomes NP-hard in this case and the reconstruction is computationally heavy [10]. Fortunately, for an underdetermined system, if there is a unique and sparse solution, the compressed sensing theory allows the recovery of that solution [11]. Because we have assumed that the fluorescent sources are sparse, it is suitable to apply the compressed sensing theory in the FMT problem. Compressed sensing is realized by incorporating the L1-norm constraint of the solution into the FMT problem. The L1-norm-constrained FMT problem can be solved by standard optimization tools, such as pursuit algorithms [12]. In recent years, several algorithms for optical

0003-6935/10/366930-08$15.00/0

tomography problems incorporating L1-norm regularization have been reported [9,13–15]. For example, in [15], the authors propose an iterated-shrinkage-based (IS-based) method for FMT, which can handle general sparse Lp-norm regularization problems. A good effort has been made to improve the computational efficiency of the method. The IS-based method belongs to the class of first-order methods, and it has been proved to have a linear convergence rate [16]. In [15], 30,000 iterations have been used to obtain satisfactory results, a number which is much larger than the dimension of the optimization problem.

In this paper, L1-norm regularization is utilized to promote the sparsity of the fluorescent sources. We treat the FMT problem as the basis pursuit problem and propose a reconstruction algorithm based on stagewise orthogonal matching pursuit (StOMP) [17]. To our best knowledge, this is the first time that the StOMP method is used for FMT reconstructions. Different from standard orthogonal matching pursuit (OMP) [18], many coefficients can be selected within one stage for StOMP, which makes StOMP run much faster than OMP. To show the merits of the proposed method, we compare it to the IS-based algorithm. From the results, it can be seen that the proposed method can obtain comparable or even slightly better results. More importantly, the proposed method was at least 2 orders of magnitude faster than the IS-based algorithm in these experiments, which makes it a practical reconstruction algorithm.

This paper is organized as follows. The proposed algorithm is presented in Section 2. In Section 3, both numerical simulations and physical experiments are conducted to evaluate the proposed algorithm. We discuss the results and conclude this paper in Section 4.

2. Method

A. Diffusion Model

In highly scattering media, the FMT model with continuous wave excitation point sources can be described by the following coupled diffusion equations [19–21]:

$$\begin{cases} -\nabla\cdot[D_x(r)\nabla\Phi_x(r)]+\mu_{ax}(r)\Phi_x(r)=\Theta\delta(r-r_l) \\ -\nabla\cdot[D_m(r)\nabla\Phi_m(r)]+\mu_{am}(r)\Phi_m(r)=\Phi_x(r)\eta\mu_{af}(r) \end{cases}^{(r\in\Omega)}, \tag{1}$$

with the Robin-type boundary conditions:

$$\Phi_{x,m}(r)+2qD_{x,m}(r)[\vec{v}(r)\cdot\Phi_{x,m}(r)]=0 \qquad (r\in\partial\Omega), \tag{2}$$

where Ω is the domain of the object, with its boundary $\partial\Omega$. Subscripts x and m denote the excitation light and the emission light, respectively. $\mu_{ax,am}$ is the absorption coefficient, and $D_{x,m}=1/3(\mu_{ax,am}+\mu'_{sx,sm})$ is the diffusion coefficient. $\mu'_{sx,sm}$ is the reduced scattering coefficient. $\Phi_{x,m}$ denotes the photon density. The excitation light is modeled as an isotropic point source $\Theta\delta(r-r_l)$, which is located one transport mean free path beneath the surface. Θ denotes the amplitude of the point source. $\vec{v}$ is the outward normal vector to the surface. q is a constant depending on the optical reflective index mismatch on the boundary [22]. $\eta\mu_{af}$ denotes the unknown fluorescent yield that is to be reconstructed.

By employing the finite element method, Eqs. (1) and (2) can be linearized and the following matrix-form equations can be obtained:

$$K_x\Phi_x=S_x, \tag{3}$$

$$K_m\Phi_m=FX, \tag{4}$$

where matrix F is obtained by discretizing the unknown fluorescent yield distribution. Vector X denotes the fluorescent yield to be reconstructed. For the excitation process, the photon density Φ_x, which is used as the energy source for the emission process, can be obtained by solving Eq. (3). For the inverse problem, based on Eq. (4), we can establish the linear relationship between the emitted fluorescence measurements Φ on the surface and the unknown fluorescent yield distribution X as follows:

$$\Phi=AX. \tag{5}$$

Detailed descriptions can be found in [8].

B. Reconstruction Based on the StOMP Algorithm

Because FMT is an ill-posed inverse problem, additional constraints on the solution should be included to regularize the problem. Considering the sparse *a priori* information of the fluorescent sources, L1-norm regularization is adopted in this study. In this case, the FMT problem can be formulated as follows:

$$\min_X E(X)=\frac{1}{2}\|AX-\Phi\|_2^2+\lambda\|X\|_1, \tag{6}$$

where λ is the regularization parameter. Here, if we consider the columns of matrix A as a set of atoms coming from a dictionary $\mathcal{D}$ and vector X as the coefficient vector, the FMT problem can be approximately regarded as the basis pursuit problem that has the following form:

$$\min\|X\|_1 \quad \text{subject to} \quad AX=\Phi. \tag{7}$$

In this case, the optimal representation X_{opt} is expected to have only a small number of significant coefficients. Various algorithms have been proposed to solve the basis pursuit problem. For instance, the OMP algorithm is a heuristic approach that starts with an empty index set. At each iteration, a single index, which maximizes an objective function, is selected and added to the index set. The algorithm stops after a specially chosen number of iterations. In this section, an FMT reconstruction algorithm

is proposed that is based on the StOMP algorithm. Different from the standard OMP method, many coefficients can be selected within one stage for StOMP, which makes StOMP run much faster than OMP.

The proposed algorithm starts with an empty index set I_0. At the nth iteration, the residual vector r_{n-1} is first calculated, which can be considered as the mismatch between the observations and the current predictions:

$$r_{n-1} = \Phi - AX_{n-1}. \tag{8}$$

Suppose A is an $m \times k$ dense matrix, then computing r_{n-1} needs $m \times k$ multiplications. This can be greatly reduced by exploring the sparsity of X_{n-1}. Suppose there are k' nonzeros in X_{n-1}, then only $m \times k'$ multiplications are actually needed, which is usually a small fraction of the original. Next we compute the residual correlations vector c_n, which can be regarded as a measure of the correlations between the atoms in A and the current residual:

$$c_n = A^T r_{n-1}. \tag{9}$$

Then hard thresholding is performed to find a small set of indices that indicate those atoms that are best for reducing the current residual:

$$S_n = \{s : s \in \bar{I}_{n-1} \wedge |c_n(s)| > t_n\}, \tag{10}$$

where $\bar{I}_{n-1}$ is the complement of set I_{n-1}, $t_n = \alpha ||c_n||_\infty$ and $\alpha \in (0,1)$ is a specially chosen threshold parameter. $\wedge$ means logical and. This is different from the OMP algorithm in which only the largest coefficient is selected within one step. Here, if S_n is an empty set, the algorithm outputs the current solution and stops. If not, S_n is merged with I_{n-1} to form the new supporting index set I_n:

$$I_n = I_{n-1} \cup S_n. \tag{11}$$

By using the supporting index set I_n, the coefficients in X can be divided into two parts: permissible and nonpermissible, and only the permissible coefficients can possibly have nonzero values. Here, we set the maximum number of the permissible coefficients to be $P_{\max}$, which is usually much smaller than the dimension of X. If $|I_n| > P_{\max}$, the algorithm outputs the current solution and stops. If not, we remove the columns of A and the corresponding elements of X whose indices are not in I_n and obtain A_{I_n} and X_{I_n}. Then the linear relationship between the observations Φ and the permissible coefficients X_{I_n} can be established as follows:

$$A_{I_n} X_{I_n} = \Phi. \tag{12}$$

Because $|I_n|$ can be much smaller than the dimension of X, Eq. (12) is often an overdetermined linear equation, and there is no exact solution in general. Therefore, we compute the least-squares solution of Eq. (12):

$$A_{I_n}^T A_{I_n} X_{I_n} = A_{I_n}^T \Phi. \tag{13}$$

In this paper, the conjugate gradient algorithm is adopted to solve Eq. (13). The iteration number is set to be $|I_n|$. Then X_n can be constructed from X_{I_n} with all the nonpermissible elements set to zero. Afterward, a new iteration of the algorithm begins. The maximum iteration number $N_{\max}$ can be specified in advance. Note that when the algorithm stops, all the negative elements in the solution are replaced with zeros. Figure 1 summarizes the proposed reconstruction algorithm.

3. Results

A. Simulation Experiments

The proposed method was first evaluated by performing reconstructions of fluorescent sources with different depths in a cylindrical phantom. This phantom had a diameter of 20 mm and a height of 20 mm. Optical parameters for the muscle region in Table 1

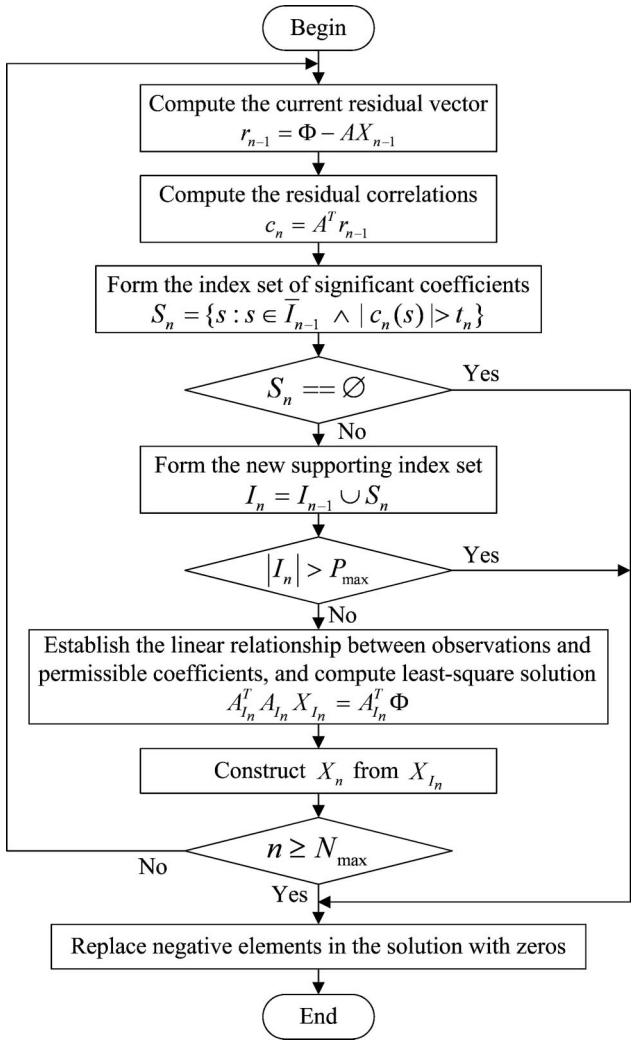

Fig. 1. Flow chart of the proposed algorithm.

Table 1. Optical Parameters of the Numerical Phantom (Unit: mm^{-1}) [23]

Region	μ_{ax}	μ'_{sx}	μ_{am}	μ'_{sm}
Muscle	0.0052	1.08	0.0068	1.03
Lung	0.0133	1.97	0.0203	1.95
Heart	0.0083	1.01	0.0104	0.99
Bone	0.0024	1.75	0.0035	1.61

were used for this phantom. Three fluorescent source configurations were considered, which are illustrated in Fig. 2. All the fluorescent sources were spherical, with a diameter of 2 mm. These fluorescent sources were centered in the $z = 0$ plane. The depths of the three sources (from the center of the source to the nearest surface) were 4, 6, and 8 mm, respectively. As can be seen from Fig. 2, the deepest source was quite near the center of the phantom. The fluorescent yield was set to be 0.5. The black dots in the cross section images of Fig. 2 represent the excitation point sources. To generate the fluorescence measurements, for each point source, the emitted fluorescence was collected from the opposite cylindrical surface within a 160° field of view. In [15], the authors have shown that by using L1 regularization, the sparsity of the fluorescent sources can be well preserved. This is especially the case when the measurement data are very limited. Therefore, to better demonstrate the sparsity-promoting characteristic of the proposed method, in our simulation experiments, only three different excitation point sources were used to generate the fluorescence measurements. Afterward, 5% Gaussian noise was added to the measurement data. For the reconstruction of the fluorescent sources, this phantom was discretized into 2978 nodes and 12,380 tetrahedron elements. In this case, there were 2978 unknowns, and the total number of measurement nodes was 1507.

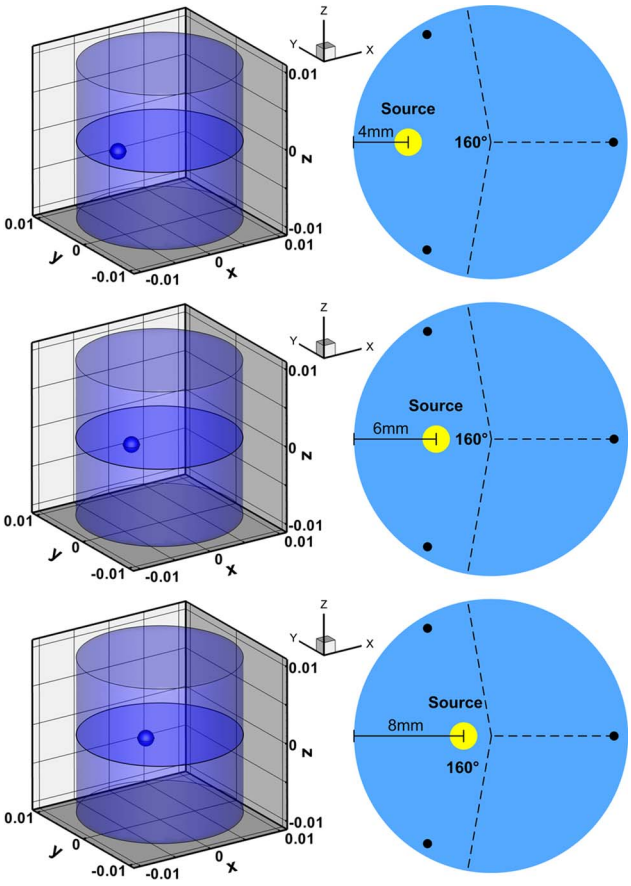

Fig. 2. (Color online) Three different fluorescent source configurations. The left column is the 3D views of the configurations, and the right column is the cross sections in the $z = 0$ plane. The black dots in the cross sections represent the excitation point sources. For each excitation point source, fluorescence was collected from the opposite cylindrical surface within a 160° field of view.

In this paper, to better evaluate the proposed algorithm, we compared it to the IS-based algorithm with L1 regularization (IS-L1), which minimized the energy function $E(X)$ in Eq. (6). For the proposed method, a maximum of 10 iterations was used. Considering the sparsity of the fluorescent sources, we set $P_{\max}$ to be 100, which was sufficiently large for these experiments. For the IS-L1 method, we set the maximum iteration number to be 30,000, which was the same as the number used in [15]. In our FMT experiments, the dimension of the optimization problem was much smaller than 30,000. Therefore, for the IS-L1 method, the second reconstruction strategy was adopted [15]. Zero vectors were used as the initial values for both methods. The tuning parameters

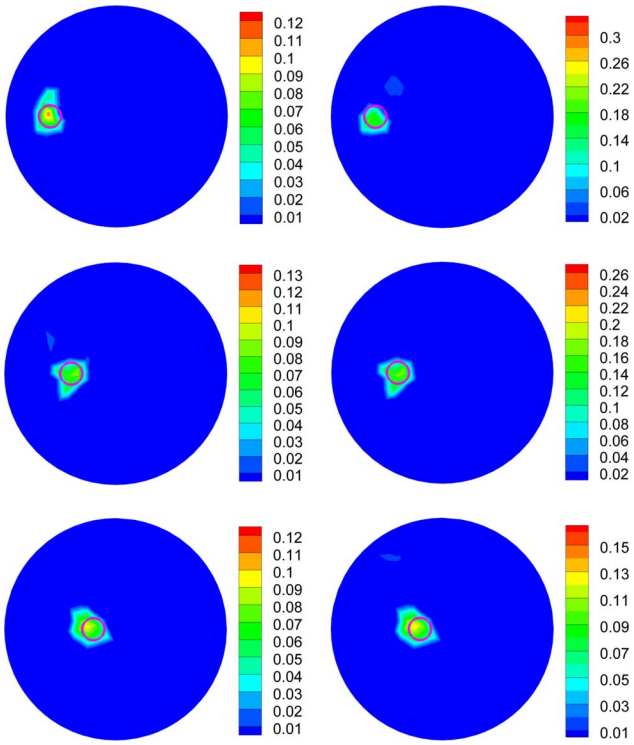

Fig. 3. (Color online) Cross sections in $z = 0$ plane of the reconstruction results for the three fluorescent sources with depths of 4 (top row), 6 (middle row), and 8 mm (bottom row), respectively. The results in the left column are from the IS-L1 method, and the results in the right column are from the proposed method. The small circles in the cross sections denote the real positions of the fluorescent sources.

Table 2. Relative Intensity Errors of the Results from the StOMP-Based and IS-L1 Algorithms

Source Depth (mm)	StOMP	IS-L1
4	34.9%	74.7%
6	44.7%	73.2%
8	65.9%	75.1%

for the proposed method and the IS-L1 method are the threshold parameter α and the regularization parameter λ, respectively. These tuning parameters were manually optimized. In our experiments, the best values for parameter α ranged between 0.7 and 0.9. In our experience, 0.8 is a proper value for most cases. Although 0.8 may not be the optimal value, it is good enough to obtain satisfactory results. Both reconstruction algorithms were implemented in C++, and all the reconstructions were performed on a personal computer with 2.33 GHz Intel Core2 duo CPU and 2 Gbytes of RAM.

Figure 3 shows the reconstruction results, which are presented by using cross sections in the $z = 0$ plane, for the three different fluorescent source configurations. From these results, it can be seen that both algorithms could obtain satisfactory fluorescent source localizations. But the reconstructed intensities were different. Table 2 presents the relative intensity errors for both algorithms, which are defined as the absolute difference between the true intensity and the maximum reconstructed intensity divided by the true intensity. From Table 2, we can see that the relative intensity errors for the proposed method were smaller. To compare the running time of the two algorithms, we set the starting point at the time when A and Φ were just obtained. Then the running time of the IS-L1 method for three different source configurations was 7.39, 6.75, and 5.07 s, respectively. Computing A^TA took up a large portion of the total reconstruction time. For the three configurations, the proposed method stopped after 3, 5, and 1 iteration, respectively. The running time of the proposed method was 0.046, 0.066, and 0.022 s, respectively. The proposed method was at least 2 orders of magnitude faster than the IS-L1 method.

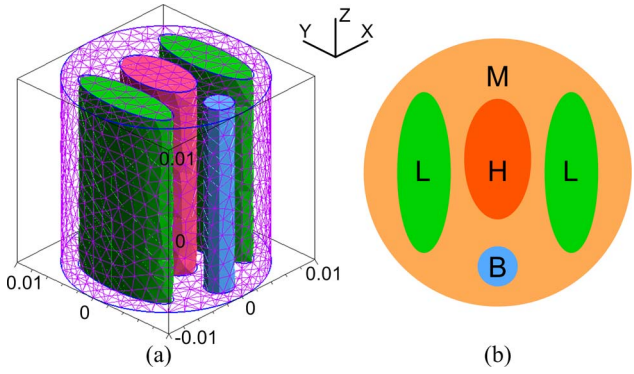

Fig. 4. (Color online) Cylindrical heterogeneous phantom with regions resembling muscle (M), lung (L), heart (H), and bone (B). (a) 3D view of the phantom. (b) Cross section of the phantom in the $z = 0$ plane.

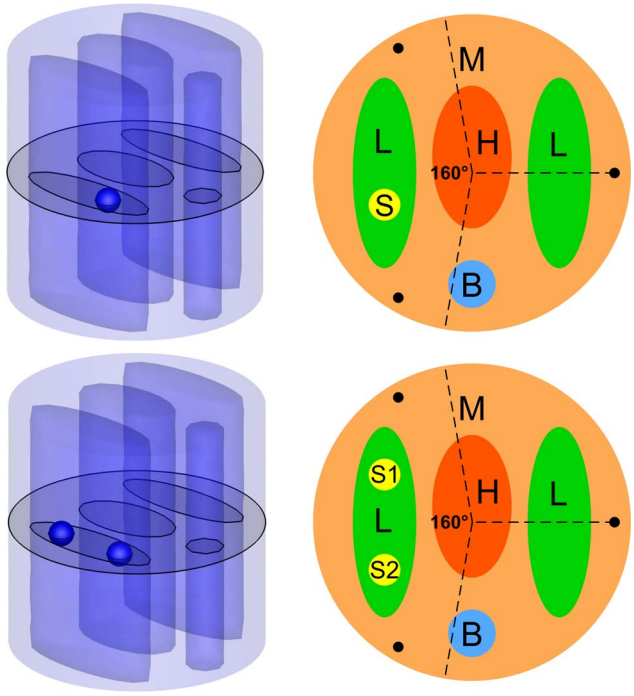

Fig. 5. (Color online) Two different fluorescent source configurations. The left column is the 3D views of the configurations, and the right column is the cross sections in the $z = 0$ plane. All the fluorescent sources were spherical with a diameter of 2 mm centered in the $z = 0$ plane. The black dots in the cross sections represent the excitation point sources. For each excitation point source, fluorescence was collected from the opposite cylindrical surface within a 160° field of view.

Next, the proposed method was further tested using a mouse-mimicking heterogeneous cylindrical phantom that contained regions resembling muscle

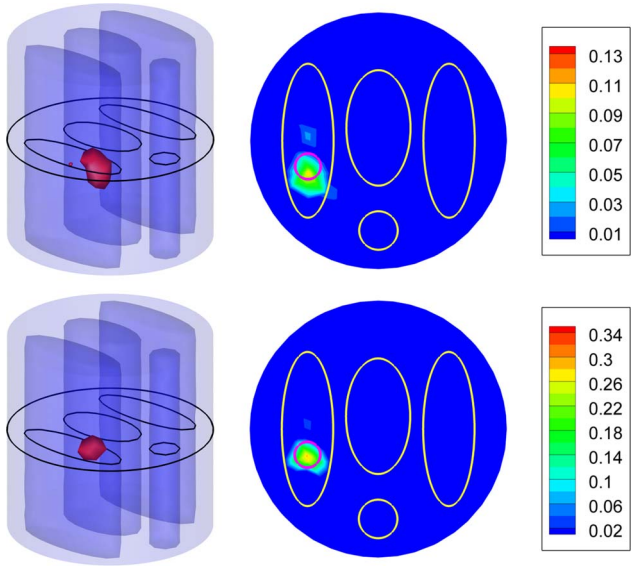

Fig. 6. (Color online) Reconstruction results from the IS-L1 method (first row) and the proposed method (second row) for one spherical fluorescent source. The left column is the isosurfaces for 30% of the maximum value. The right column is the cross sections in the $z = 0$ plane. The small circles in the left lung regions of the cross sections denote the real positions of the fluorescent sources.

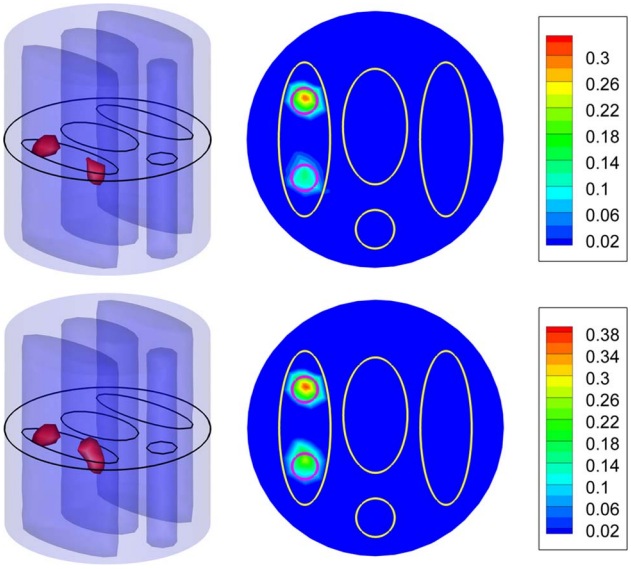

Fig. 7. (Color online) Reconstruction results from the IS-L1 method (first row) and the proposed method (second row) for two spherical fluorescent sources. The left column is the isosurfaces for 30% of the maximum value. The right column is the cross sections in the $z = 0$ plane. The small circles in the left lung regions of the cross sections denote the real positions of the fluorescent sources.

(M), lung (L), heart (H) and bone (B), which has been used in [15]. The optical parameters adopted in [15] were assigned to each of the four regions; see Table 1. This phantom was 20 mm in diameter and 20 mm in height. Figure 4 shows the 3D view of the phantom and its cross section in the $z = 0$ plane. Two fluorescent source configurations were designed to test the proposed method, which are illustrated in Fig. 5. The size and the fluorescent yield of the sources were the same with the ones in the previous experiments. Still, only three different excitation point sources were used. This phantom was discretized into 2710 nodes and 13,316 tetrahedron elements. In this case, there were 2710 unknowns, and the total number of measurement nodes was 839.

Figures 6 and 7 present the reconstruction results for the two different fluorescent source configurations. Both isosurfaces for 30% of the maximum value and cross sections in the $z = 0$ plane are provided. Still, both algorithms could obtain satisfactory localizations. As can be seen in Table 3, the relative intensity errors for the proposed method were smaller. The running time of the IS-L1 method for two different configurations was 3.69 and 4.15 s, respectively. For the two configurations, the proposed method stopped after three and five iterations, respectively.

Table 3. Relative Intensity Errors of the Results in the Heterogeneous Simulation Experiments

Configuration	Source No.	StOMP	IS-L1
One Source	S	27.9%	72.4%
Two Sources	S1	20.1%	34.4%
	S2	44.8%	59.8%

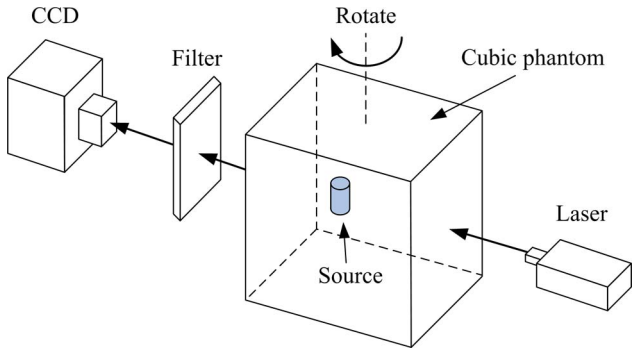

Fig. 8. (Color online) Sketch of the imaging system.

The running time was 0.023 and 0.032 s, respectively. The proposed method was at least 2 orders of magnitude faster.

B. Physical Experiments

In this subsection, a physical phantom experiment was conducted by employing a noncontact, continuous wave imaging system in the transillumination mode, which has been adopted in [15]. A sketch of the system is shown in Fig. 8. When performing reconstructions of the experimental data, the emitted fluorescence distribution on the surface of the physical phantom should first be calculated based on the captured fluorescence image. To avoid the errors in this procedure, a cubic phantom was used in this experiment. In this case, there was a point-to-point correspondence between the surface of the phantom and the captured fluorescence image, and the errors could be minimized then. The cubic phantom with a side length of 20 mm was made of polyoxymethylene. A cylindrical hole of 2.5 mm in diameter filled with Cy5.5 solution was used as the fluorescent source; see Fig. 9. The height of the cylindrical fluorescent source was 2 mm, and the center was at (2.5, −2.5, 1 mm). The optical parameters of this phantom for both the excitation and emission wavelengths, which

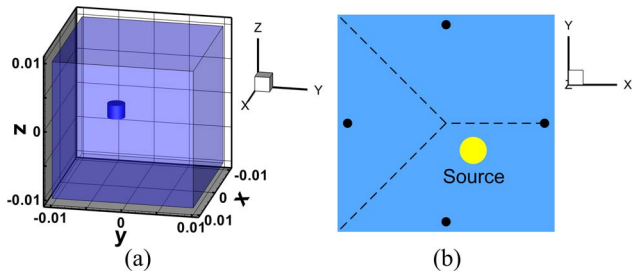

Fig. 9. (Color online) Cubic phantom with one cylindrical fluorescent source. (a) 3D view of the phantom and the source. (b) Cross section in the $z = 0$ plane. The black dots in (b) represent the excitation point sources.

Table 4. Optical Parameters of the Cubic Phantom

Wavelength (nm)	μ_a (mm^{-1})	μ_s' (mm^{-1})
671	0.00029	1.08
700	0.00051	1.11

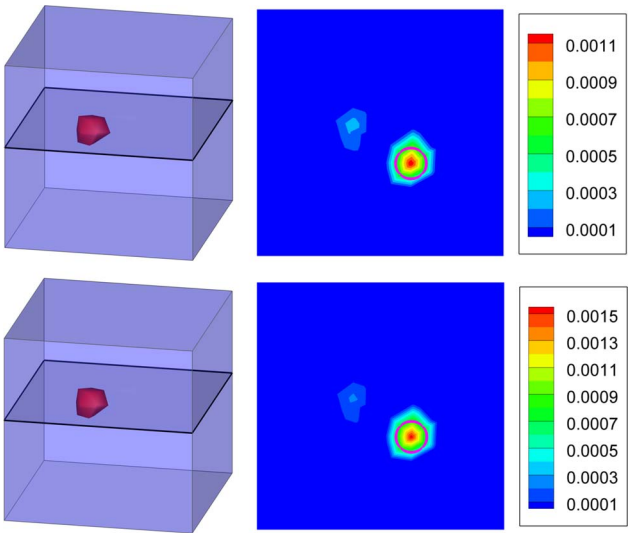

Fig. 10. (Color online) Reconstruction results from the IS-L1 method (first row) and the proposed method (second row), respectively. The left column is the isosurfaces for 30% of the maximum value. The right column is the cross sections in the $z = 1$ mm plane. The small circles in the cross sections denote the real positions of the fluorescent sources.

were determined by diffuse optical tomography, are presented in Table 4. Four different excitation point sources in the $z = 0$ plane, which are illustrated in Fig. 9(b), were used to generate the fluorescence measurements. The emitted fluorescence was captured from the opposite side. For the reconstruction of the fluorescent source, this phantom was discretized into 2705 nodes and 11,239 tetrahedron elements. In this case, there were 2705 unknowns, and the total number of measurement nodes was 1054.

Figure 10 shows the reconstruction results from the two methods. Both isosurfaces for 30% of the maximum value and cross sections in the $z =$ 1 mm plane are provided. As can be seen in Fig. 10, both methods could obtain satisfactory fluorescent source localizations, though some insignificant artifacts existed. This demonstrates the applicability of the two methods under badly ill-posed situations. The running time of the IS-L1 method was 3.82 s. However, only three iterations were needed for the proposed method, and the running time was 0.022 s. The proposed method was at least 2 orders of magnitude faster when compared with the IS-L1 method.

4. Discussion and Conclusion

In this paper, the FMT problem with sparsity-promoting L1-norm regularization is treated as the basis pursuit problem, and a reconstruction algorithm based on the StOMP is proposed. At each iteration, this algorithm seeks a small index set that indicates those atoms that are best for reducing the current residual. Then the current supporting (permissible) index set is updated by merging the newly selected index set. This can be considered as a kind of *a posteriori* permissible region strategy. Based on this, a new least-squares problem, with a greatly reduced order compared to the original problem, is formed between the observations and the permissible coefficients. The conjugate gradient algorithm is adopted to solve the least-squares problem. Then the new solution can be constructed from the permissible coefficients. To evaluate the proposed algorithm, we compare it to the IS-L1 algorithm. Reconstruction results show that the proposed method could obtain comparable or even slightly better results. More importantly, in these experiments, the proposed method was at least 2 orders of magnitude faster than the IS-L1 algorithm, which makes it a practical FMT reconstruction algorithm.

In the proposed method, the regularization parameter is the threshold parameter α. Besides, there are two other parameters in this method, the maximum number of the permissible coefficients $P_{\max}$ and the maximum iteration number $N_{\max}$. In this paper, $P_{\max}$ was set to be 100, which was much smaller than the total number of unknowns. This is based on the assumption that the fluorescent sources should be sparse. In our experiments, the numbers of the nonzero coefficients in the reconstruction results were still much smaller than 100. In fact, we did not try to optimize $P_{\max}$, and we found that the reconstruction results were not sensitive to the change of $P_{\max}$. Because different FMT experiments have different numbers of unknowns, we can set $P_{\max}$ to be a certain portion of the total number of unknowns when the proposed method is taken into practical use. For the parameter $N_{\max}$, we set it to be 10, which was the same with the value used in [17]. In our experiments, all the reconstructions stopped within 10 iterations. Still, we did not try to optimize $N_{\max}$. In our experience, 10 iterations are sufficient for most cases. For the threshold parameter α, although we have not provided a way to determine it automatically, we have found that 0.8 is a proper value for most cases. From the above analysis, we can see that although there are three parameters in the proposed method, we generally do not need to change them. From this point of view, the proposed method is more stable than the IS-based method.

For optical tomography problems, the diffusion approximation to radiative transfer equation has been extensively applied to model the light transport in biological tissue. The advantage of the diffusion equation is that it is computationally efficient. Besides, it has an explicit physical meaning. However, the diffusion equation is not applicable in the regions with high absorption. To resolve the problem, several improved models have been adopted in recent years, for example, the simplified spherical harmonics approximation (SP_N). The proposed method can be applied in these improved models with little modifications.

In conclusion, we have proposed an efficient reconstruction algorithm for FMT based on the StOMP algorithm. Future work will be focused on *in vivo* mouse studies using the proposed algorithm.

This paper is supported by the Project for the National Basic Research Program of China (973) under

grant 2011CB707700, the Knowledge Innovation Project of the Chinese Academy of Sciences (CAS) under grant KGCX2-YW-907, the National Natural Science Foundation of China (NSFC) under grants 81027002 and 81071205, the Hundred Talents Program of the CAS, and the Science and Technology Key Project of the Beijing Municipal Education Commission under grant KZ200910005005.

†These authors contributed equally to this work.

References

1. V. Ntziachristos, J. Ripoll, L. V. Wang, and R. Weissleder, "Looking and listening to light: the revolution of whole-body photonic imaging," Nat. Biotechnol. **23**, 313–320 (2005).
2. J. K. Willmann, N. van Bruggen, L. M. Dinkelborg, and S. S. Gambhir, "Molecular imaging in drug development," Nat. Rev. Drug Discov. **7**, 591–607 (2008).
3. J. Tian, J. Bai, X. Yan, S. Bao, Y. Li, W. Liang, and X. Yang, "Multimodality molecular imaging," IEEE Eng. Med. Biol. Mag. **27**, 48–57 (2008).
4. V. Ntziachristos, "Fluorescence molecular imaging," Annu. Rev. Biomed. Eng. **8**, 1–33 (2006).
5. W. Bangerth and A. Joshi, "Adaptive finite element methods for the solution of inverse problems in optical tomography," Inverse Probl. **24**, 034011 (2008).
6. Y. Tan and H. Jiang, "Diffuse optical tomography guided quantitative fluorescence molecular tomography," Appl. Opt. **47**, 2011–2016 (2008).
7. F. Gao, H. Zhao, L. Zhang, Y. Tanikawa, A. Marjono, and Y. Yamada, "A self-normalized, full time-resolved method for fluorescence diffuse optical tomography," Opt. Express **16**, 13104–13121 (2008).
8. X. Song, D. Wang, N. Chen, J. Bai, and H. Wang, "Reconstruction for free-space fluorescence tomography using a novel hybrid adaptive finite element algorithm," Opt. Express **15**, 18300–18317 (2007).
9. P. Mohajerani, A. A. Eftekhar, J. Huang, and A. Adibi, "Optimal sparse solution for fluorescent diffuse optical tomography: theory and phantom experimental results," Appl. Opt. **46**, 1679–1685 (2007).
10. I. F. Gorodnitsky and B. D. Rao, "Sparse signal reconstruction from limited data using FOCUSS: a re-weighted minimum norm algorithm," IEEE Trans. Signal Process. **45**, 600–616 (1997).
11. E. J. Candes, J. K. Romberg, and T. Tao, "Stable signal recovery from incomplete and inaccurate measurements," Commun. Pur. Appl. Math. **59**, 1207–1223 (2006).
12. D. L. Donoho and X. Huo, "Uncertainty principles and ideal atomic decomposition," IEEE Trans. Inf. Theory **47**, 2845–2862 (2001).
13. Y. Lu, X. Zhang, A. Douraghy, D. Stout, J. Tian, T. F. Chan, and A. F. Chatziioannou, "Source reconstruction for spectrally-resolved bioluminescence tomography with sparse a priori information," Opt. Express **17**, 8062–8080 (2009).
14. N. Cao, A. Nehorai, and M. Jacob, "Image reconstruction for diffuse optical tomography using sparsity regularization and expectation-maximization algorithm," Opt. Express **15**, 13695–13708 (2007).
15. D. Han, J. Tian, S. Zhu, J. Feng, C. Qin, B. Zhang, and X. Yang, "A fast reconstruction algorithm for fluorescence molecular tomography with sparsity regularization," Opt. Express **18**, 8630–8646 (2010).
16. M. Elad, B. Matalon, and M. Zibulevsky, "Coordinate and subspace optimization methods for linear least squares with non-quadratic regularization," Appl. Comput. Harmon. Anal. **23**, 346–367 (2007).
17. D. L. Donoho, Y. Tsaig, I. Drori, and J. L. Starck, "Sparse solution of underdetermined linear equations by stagewise orthogonal matching pursuit," Tech. Rep. 2006-02 (Stanford Department of Statistics, 2006).
18. J. A. Tropp and A. C. Gilbert, "Signal recovery from random measurements via orthogonal matching pursuit," IEEE Trans. Inf. Theory **53**, 4655–4666 (2007).
19. Y. Tan and H. Jiang, "DOT guided fluorescence molecular tomography of arbitrarily shaped objects," Med. Phys. **35**, 5703–5707 (2008).
20. D. Wang, X. Liu, Y. Chen, and J. Bai, "A novel finite-element-based algorithm for fluorescence molecular tomography of heterogeneous media," IEEE Trans. Inf. Technol. Biomed. **13**, 766–773 (2009).
21. G. Y. Panasyuk, Z. Wang, J. C. Schotland, and V. A. Markel, "Fluorescent optical tomography with large data sets," Opt. Lett. **33**, 1744–1746 (2008).
22. M. Schweiger, S. R. Arridge, M. Hiraoka, and D. T. Delpy, "The finite element method for the propagation of light in scattering media: boundary and source conditions," Med. Phys. **22**, 1779–1792 (1995).
23. A. X. Cong and G. Wang, "A finite-element-based reconstruction method for 3D fluorescence tomography," Opt. Express **13**, 9847–9857 (2005).